UCRL-JRNL-406423

LAWRENCE
LIVERMORE
NATIONAL
LABORATORY

Large-Spot Material Interactions with a High-Power Solid-State Laser Beam

C. D. Boley, S. N. Fochs, and A. M. Rubenchik

August 6, 2008

Journal of Directed Energy

This document was prepared as an account of work sponsored by an agency of the United States government. Neither the United States government nor Lawrence Livermore National Security, LLC, nor any of their employees makes any warranty, expressed or implied, or assumes any legal liability or responsibility for the accuracy, completeness, or usefulness of any information, apparatus, product, or process disclosed, or represents that its use would not infringe privately owned rights. Reference herein to any specific commercial product, process, or service by trade name, trademark, manufacturer, or otherwise does not necessarily constitute or imply its endorsement, recommendation, or favoring by the United States government or Lawrence Livermore National Security, LLC. The views and opinions of authors expressed herein do not necessarily state or reflect those of the United States government or Lawrence Livermore National Security, LLC, and shall not be used for advertising or product endorsement purposes.

Large-Spot Material Interactions with a High-Power Solid-State Laser Beam

C. D. Boley[1], S. N. Fochs[2], and A. M. Rubenchik[3]
Lawrence Livermore National Laboratory
Livermore, CA 94551

We study the material interactions produced by the beam of a 25-kW solid-state laser, in experiments characterized by relatively large spot sizes (~3 cm) and the presence of airflow. The targets are iron or aluminum slabs, of thickness 1 cm. In the experiments with iron, we show that combustion plays an important role in heating the material. In the experiments with aluminum, we observe a sharp transition from no melting to complete melt-through as the intensity on target increases. A layer of paint greatly reduces the requirements for melt-through. We explain these effects and incorporate them into an overall computational model.

Keywords: solid-state laser, high average power, large spot size, airflow, combustion.

Nomenclature

C	specific heat
I	laser intensity
T	temperature
T_c	combustion initiation temperature
U_0	wind speed
x_o	thickness of oxide layer
α	optical absorptivity
η	shear viscosity
κ	thermal conductivity
ρ	density
σ	shear stress

1. Introduction

Solid-state lasers with high average power are of great current interest. Our laboratory at LLNL has been developing such lasers for defense applications during the last decade. Here we are concerned with a device[9,10] containing four diode-pumped ceramic Nd:YAG slabs, which produces approximately 25 kW of time-average power at a wavelength of 1.053 μm. Routine

[1]E-mail address: boley1@llnl.gov; telephone: (925) 423-7365; fax: (925) 423-7186.
[2]Current address: Metal Improvement Company, Livermore, CA 94551; e-mail address: Scott_Fochs@metalimprovement.com, telephone: (925) 960-1090.
[3]E-mail address: rubenchik1@llnl.gov; telephone: (925) 422-6131.

This work performed under the auspices of the U.S. Department of Energy by Lawrence Livermore National Laboratory under Contract DE-AC52-07NA27344

operation for 10 seconds has been demonstrated. The laser operates at a pulse repetition rate of 200 Hz, producing pulses of energy about 125 J and length about 0.5 ms, for a duty factor of about 10%. With the addition of another slab and an increased diode duty factor, the laser has also achieved 67 kW for 0.25 s (as limited by diode capabilities). During lasing operations, the laser stores waste heat in the solid-state slabs. In field applications, the hot slabs would be interchanged with cool slabs and rapidly cooled.

Our laser power corresponds to the power on target for a tactical defense system having approximately twice that power (50 kW), since projected losses due to the beam director and propagation are typically of order 50%. The spot size (~3 cm) is representative of that expected for many field targets. To simulate field conditions, air flow of about 100 m/sec was used in the most of experiments. Hence our results are applicable for the description of laser-matter interaction of more practical and powerful systems.

We have explored the material interactions of our lasers, including high-explosive initiation, at some length[2-5]. Since the thermal conduction length between pulses is small compared to typical target dimensions, the macroscopic heat distribution is readily seen to be governed by the time-average power, as opposed to the peak power [5] (the latter is, of course, about 10 times the former). Our predictive capability is embodied in a computational model. With this model, devices operating near 100 kW have been projected to be effective in defense against tactical projectiles[2,4,5].

The goal of the present paper is twofold: to study laser-matter interactions under conditions approximating those in the field (large spot size, intensity below vaporization threshold, airflow); and to use the experiments to benchmark and calibrate our code and to include the new physics effects in modeling.

Laser-matter interactions for defense applications have been studied since at least the 1970s, and a great deal of data has been collected (see, e.g., the extensive review[7] and also the lectures[1]). The data are sensitive to the laser wavelength, pulse duration, laser intensity, materials, and so forth. Because of the impetus for a 100-kW solid-state laser, studies such as ours of large-spot, multi-kW interactions at 1 μm are particularly timely.

Our experiments employed thick (1 cm) iron and aluminum coupons. For iron, this approximates the shell thickness of some mortars. For Al, this is related to the wall thickness of wing fuel tanks. The beam footprint was square, with nearly uniform intensity over the spot. Examination of the laser imprint after several pulses showed no visible patterns. According to calorimetry, the pulse-to-pulse energy varied by less than 5%. In all experiments, the time-average power was 25 kW and the irradiation time was 5 s. The experimental setup near the target is shown in Fig. 1.

In the case of iron, we demonstrate that, under these conditions, combustion plays an important role in facilitating material heating. This was also suggested by earlier experiments at lower power[3]. For aluminum, we find that target damage sharply changes with increased intensity. At about 3 kW/cm^2, no cratering or melting is observed. At twice this intensity, however, the coupon rapidly melts through. This effect is explained by the large thermal conductivity of Al. The behavior is altered by a paint layer, which serves to increase the absorption. As a result, Al targets differ from iron in sensitivity to paint. We show that our simulations are consistent with these observations.

2. Interactions with Iron Coupons

We begin by describing the irradiation of iron coupons. These were made from mild steel 1020. The coupon size (5x7.5 cm^2) was sufficiently large to eliminate boundary effects. The spot

size was 3x3 cm^2, corresponding to an average intensity of about 2.8 kW/cm^2. At this intensity, the energy losses to vaporization are insignificant. The temperature history at the rear center of a coupon was recorded with a thermocouple. Experiments were conducted for three cases: (1) no flow past the surface; (2) air flow at about 100 m/s; and (3) nitrogen flow at this speed. Melt-through was observed with airflow but not with nitrogen flow or in the absence of flow. The difference between no flow and airflow is evident in the coupon photographs of Fig. 2. Note the viscous dripping under gravity in the former case.

More detailed information is revealed in the thermocouple readings shown in Figure 3. This shows that there is a striking difference between airflow and nitrogen flow. While each involves melt removal by the wind, the temperature is visibly enhanced by airflow. From measurements of the removed material, we estimated Q*, the amount of laser energy to remove unit mass of material. We obtain Q* = 5.7 kJ/g without flow. With nitrogen flow, we have Q* = 4.7 kJ/g, while with air flow we have Q* < 3.2 kJ/g (an upper bound, since melt-through was achieved). The decrease from no flow to nitrogen flow is explained by melt removal. The decrease from nitrogen and to air flow is attributed to combustion. Here we wish to explain the difference between airflow and nitrogen flow in more detail. To do so, we turn to our interaction model and add combustion effects.

Our model[5] describes physical processes within an irradiated target. After absorption of the incident laser energy, heat is conducted through the target via the heat conduction equation,

$$\rho C \partial T / \partial t = \nabla \cdot \kappa \nabla T + S , \qquad (1)$$

where S is a source term particular to the problem. Melt removal and wind cooling are included in the model. Calculations are performed in two-dimensional (r,z) symmetry, relative to the beam centerline. The model accesses a database of temperature-dependent material properties,

including the heat capacity C, the thermal conductivity κ, and the absorptivity at the laser wavelength.

We have added combustion effects to this model by considering a thin oxide layer of thickness x_o, situated on a melt layer. This enters into the boundary condition for the heat conduction equation via

$$\kappa \frac{\partial T}{\partial z} = \alpha I + W_c \dot{x}_o, \tag{2}$$

where α is the temperature-dependent surface absorptivity and W_c is the latent heat of the combustion reaction, per volume. The z-axis is oriented such that the temperature gradient is ordinarily positive. The growth of the oxide layer is governed by the equation[8]

$$\dot{x}_o = (D / x_o) \exp(-T_c / T), \tag{3}$$

where T_c is the initiation temperature and D is an empirical parameter. This equation describes the oxygen diffusion through the oxide layer. The self-consistent description of laser-induced combustion has been the subject of many studies[8]. In our case, the situation is greatly simplified by the fact that the wind removes the melt layer along with the oxide layer. Thus the oxide thickness and the rate of oxidation are determined primarily by wind effects rather than by complex thermochemical reactions. Eq. (3) is to be evaluated at the time required for melt removal, which is of order a/u, where a is the spot size and u is the melt speed at the melt surface. The latter, in turn, is of order $\sigma h / \eta$, where h is the melt depth, η is the shear viscosity of the melt, and σ is the shear stress at the surface. We assume a turbulent boundary layer in which the shear stress is given by the von Karman expression[6] $\sigma = c \rho_0 U_0^2$, where ρ_0 and U_0 are the density and speed, respectively, of the wind. The overall factor c is insensitive to details of

the flow and depends logarithmically on the flow velocity. Finally, then, the boundary condition (2) takes the form

$$\kappa \frac{\partial T}{\partial z} = \alpha I + Q_c U_0 \exp(-T_c / 2T) . \tag{4}$$

Thus the heating flux due to combustion, as summarized in the last term, is proportional to the wind speed and increases exponentially with the surface temperature. The parameter Q_c comprises both material and flow parameters. Unfortunately, the parameters Q_c and T_c are not available in the literature. Therefore we resorted to fitting them from our data. The model neglects the change of oxide reflectivity and also the effect of flow structure on melt removal. We hope that the limits of applicability can be ascertained by more detailed experiments.

Figure 4 shows the thermocouple temperature as calculated by this model, with Q_c = (0.8 kW/cm^2)/(10^4 cm/s) and T_c = 4000 K. It agrees well with experiment. (In such runs, we used a fixed T_c, as estimated from energetics, and varied Q_c for the best visual fit. On this basis, the quoted Q_c is estimated to be accurate within about 20%.) Overall, combustion adds approximately 35% to the deposited energy for our experiment. The code cannot reliably predict the final shape of the cavity, since this is determined in part by gravity effects and lip motion.

In Fig. 5 we show the result of a calculation with wind but without combustion. As expected from our picture, this agrees with the laboratory result for nitrogen flow.

The modified boundary condition (4) makes it possible to estimate the effect of combustion on lethality involving rapid cook-off. Of course this typically occurs before the material is melted through. The results will be published separately.

Our experiments were performed with a wind speed of about 100 m/s. Unfortunately, the speed could not be increased. From Eq. (4), we predict that the role of combustion should

increase with projectile speed. Thus it would be very interesting to do experiments with a higher wind speed, as would be pertinent, say, for some rockets.

3. Interactions with Aluminum Coupons

Next we turn to the irradiation of aluminum coupons. These were made from the alloy Al 6061. Again the coupon size (12.5x12.5 cm^2) was sufficient to eliminate boundary effects. As in the previous section, the coupon thickness was 1 cm. The temperature history at the rear center of a coupon was recorded with a thermocouple. Combustion is not important for aluminum, since the oxide layer is sufficiently dense to suppress combustion.

Before we present the results, let us discuss what we expect to observe. For iron coupons, the temperature typically has a strong gradient near the edge, owing to the relatively low thermal conductivity. Consequently, a thin melted layer is continuously removed by the wind. A painted layer will be removed in the very beginning of the laser target interaction. As a result, paint would not be expected to have a significant effect on laser penetration[8].

The situation with Al is different. The thermal conduction time through the coupon is about 0.25 sec, so the temperature profile will be practically uniform across the coupon. When the front surface starts to melt, the rear surface is also close to the melting point. As a result, one can expect a sharp change in the behavior with increase in intensity, for a given irradiation time. When the intensity is insufficient to melt the surface, the laser pulse causes essentially no surface modification. Once the power is high enough to start melting, though, practically the entire irradiated slab is melted and removed by the wind. Thus we expect a sharp transition from absence of an effect to melt-through as the laser intensity increases. The experiments are consistent with this description.

Figure 6 shows the experimental temperature trace for a spot size of 2.8x2.8 cm^2, corresponding to an intensity of about 3.2 kW/cm^2. During the irradiation time, the temperature grows to a maximum of about 400 C, with no melting. Also shown is the model calculation, which agrees well with the data throughout the experiment. The right-hand plot shows the temperature distribution at maximum. This clearly exhibits two-dimensional effects, owing to the large thermal conductivity. To fit the data we used a mildly temperature-dependent absorptivity which increased from 0.13 at room temperature to 0.24 at the melting point. The linear growth with temperature is consistent with the Drude model[8]. The former value exceeds the normally quoted value of a few percent for pure aluminum, because of surface roughness, but less then the cited value of 0.2 for Al 2024 alloys[1].

In the next experiment, the spot size on the coupon was decreased to 2x2 cm^2. As shown in Fig. 7, both experiment and model now give material melt-through at about 3 s. This suggests that our code description of melt removal provides a reasonable description of the experiments.

The presence of paint greatly changes the interaction with an aluminum target. Paints have a complicated composition and are available in many varieties, but in most cases the absorptivity of the painted surface is much higher than bare aluminum. In an elementary model, paint acts as a thin layer with a high absorptivity and a low thermal conductivity. To see its effect on aluminum, we irradiated a painted coupon, with a spot size of 3x3 cm^2, for 5 s. The paint was a dull grey. It was a commercial aerosol spray, without primer. As we noted earlier, a slightly smaller spot size, 2.8x2.8 cm^2, failed to produce melting. The painted coupon, however, absorbed appreciably more energy and melted through somewhat after 2 s, as shown in Fig. 8. (The thermocouple failed at 2 s, because of the loss of material strength below melting temperature.) This experiment suggests that the paint survived approximately to the point at

which the aluminum began to melt. Because at this moment the temperature profile across the target is close to the melting point, a painted layer should greatly decrease the power required to penetrate an aluminum target.

Also shown in Fig. 8 is the result of a 2D thermal calculation, in which the paint was treated as a 200-μm layer with an absorptivity of 0.5, a thermal conductivity of 0.08 W/(cm K), and a volume specific heat of 1 J/(cm^3 K). The thermal conduction time across the paint layer, about 1 ms, is short compared to the time scale of the experiment. The paint was assumed to decompose at 500 C. Numerically, a paint cell was removed when it reached this temperature. The temperature trace is reasonably close to experiment, as shown in Fig. 8. These confirm that our simple model of this paint may be adequate. The paint model is admittedly idealized, since, for example, carbonization typically increases the absorptivity. However, we would not expect the results to be very sensitive to such refinements.

4. Conclusions

We have described experiments and modeling concerning the interactions of a high-power solid-state laser with target materials. The laser delivered 25 kW for 5 s, on coupons of iron and aluminum having a thickness of 1 cm. The spot sizes were relatively large, about 3x3 cm^2. Airflow at about 100 m/s was present.

For an iron coupon, we showed that combustion plays an important role in adding to the material heating. This effect was absent in nitrogen flow. For aluminum, we found a strong dependence on the incident laser intensity. At approximately 3.2 kW/cm^2, no melting was observed, because of efficient lateral heat conduction. At about 6.2 kW/cm^2, however, the coupon rapidly melted through. This behavior was explained in terms of rapid heat conduction

along the axial direction. Paint was observed to increase appreciably the absorption and thus should decrease the power needed for melt-through.

Finally, we showed that all these results are reproduced by a comprehensive computational model, which includes the temperature-dependent thermal conduction, melting and melt removal by the wind, wind cooling, and iron combustion. With the modifications calibrated by these experiments, the model can be used for further applications.

Acknowledgments

We are pleased to acknowledge our debt to R. M. Yamamoto. This work performed under the auspices of the U.S. Department of Energy by Lawrence Livermore National Laboratory under Contract DE-AC52-07NA27344.

References

[1]Beraun, J. E., "Laser Materials Effects," Short Course, Fifth Annual Directed Energy Symposium, Monterey, CA, Nov. 12, 2002; Beraun, J. E., and J. Evanoff, "Laser Effects and Vulnerability Assessment Process," Short Course, Sixth Annual Directed Energy Symposium, Albuquerque, NM, October 20, 2003.

[2]Boley, C. D., S. N. Fochs, and A. M. Rubenchik, "Lethality of a High-Power Solid-State Laser," Ninth Annual Directed Energy Symposium, Albuquerque, NM, Oct. 30 – Nov. 3, 2006.

[3]Boley, C. D., and A. M. Rubenchik, "Modeling of High-Energy Pulsed Laser Interactions with Coupons," University of California, UCRL-ID-151857, Feb. 6, 2003.

[4]Boley, C. D., and A. M. Rubenchik, "Lethality of High-Power Solid-State Lasers on High-Explosive Targets," Eighth Annual Directed Energy Symposium, Lihue, HI, Nov. 14-18, 2005.

[5]Boley, C. D., and A. M. Rubenchik, "Modeling of Antimortar Lethality by a Solid-State Heat-Capacity Laser," J. Directed Energy **2**, 97-106 (2006).

[6]Landau, L. D., and E. M. Lifshitz, "Fluid Mechanics," Pergamon Press, 1978.

[7]Physical Sciences, Inc. (W. T. Laughlin, H. H. Legner, M. G. Miller, E. R. Pugh, and G. A. Simons), "Laser Materials Effects and Lethality Handbook," PSI-1302/TR-1615 (1999).

[8]Prokhorov, A. M., V. I. Konov, I. Ursu, and I. N. Mihailescu, "Laser Heating of Metals," Adam Hilger, 1990.

[9]Soules, T. F., *et al*., "Ceramic Nd:YAG – Current Material of Choice for SSHCL," Eighth Annual Directed Energy Symposium, Lihue, HI, Nov. 14-18, 2005.

[10]Yamamoto, R. M., *et al.*, "Laser Performance of the Solid-State Heat-Capacity Laser (SSHCL)," Ninth Annual Directed Energy Symposium, Albuquerque, NM, Oct. 30 – Nov. 3, 2006.

Figure Captions

Fig. 1. Experimental setup, immediately after irradiation of a target. The laser is out of view, to the lower right. The designated elements are:

(a) Beam path;

(b) Blower assembly;

(c) Target (in this case, a metal sheet with a 13x13 cm^2 spot size);

(d) Coupon pieces on a screen;

(e) Suction assembly.

Fig. 2. Iron coupons after irradiation experiments. Left: no flow; right: airflow. The beam spot size is 3x3 cm^2.

Fig. 3. Thermocouple readings for the iron coupons. The beam was turned off at 5 s.

Fig. 4. Left: Comparison of experimental and calculated temperatures on the rear center of an iron coupon, with airflow. Right: Calculated hole profile immediately before breakthrough. A circularly symmetric geometry is used.

Fig. 5. Comparison of experimental and calculated temperatures on the rear center of an iron coupon, with nitrogen flow.

Fig. 6. Irradiation of a 1-cm aluminum coupon by 25 kW for 5 s, with a spot size of 2.8x2.8 cm^2. Left: Temperature trace of a thermocouple on the rear center, along with the model calculation. Right: Calculated temperature distribution immediately before the beam is turned off. The beam enters from the right.

Fig. 7. Temperature trace at the rear center of an aluminum coupon, during irradiation with a spot size of 2x2 cm^2.

Fig. 8. Black line: Thermocouple trace for the irradiation of a 1-cm painted aluminum coupon by 25 kW for 5 s, with a spot size of 3x3 cm^2. The thermocouple failed at 2 s. The red line gives the model prediction. The blue line gives the temperature trace for a 2.8x2.8 cm^2 spot with no paint, from Fig. 6.

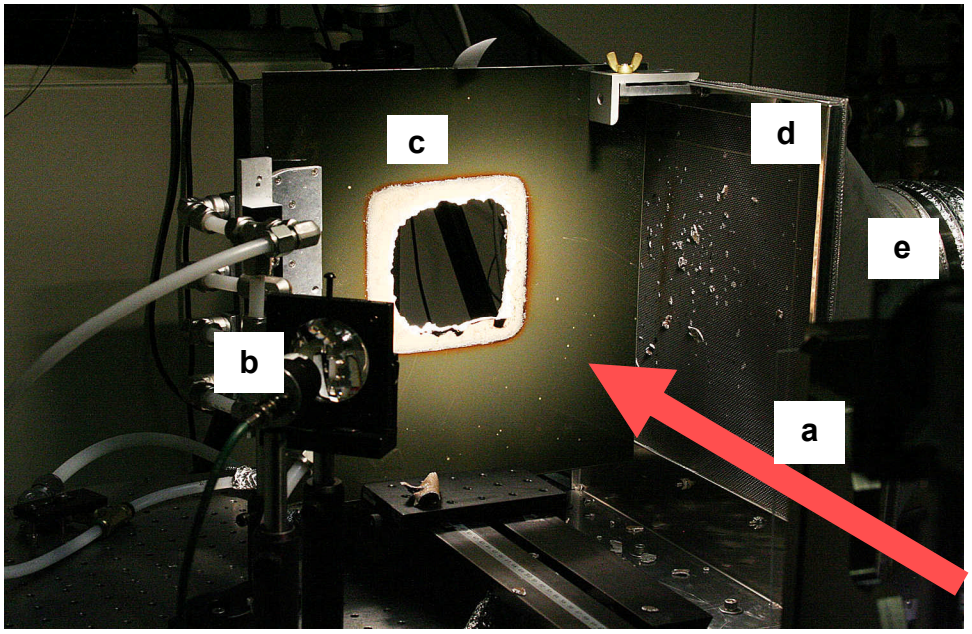

Fig. 1. Experimental setup, immediately after irradiation of a target. The laser is out of view, to the lower right. The designated elements are:

(a) Beam path;

(b) Blower assembly;

(c) Target (in this case, a metal sheet with a 13x13 cm^2 spot size);

(d) Coupon pieces on a screen;

(e) Suction assembly.

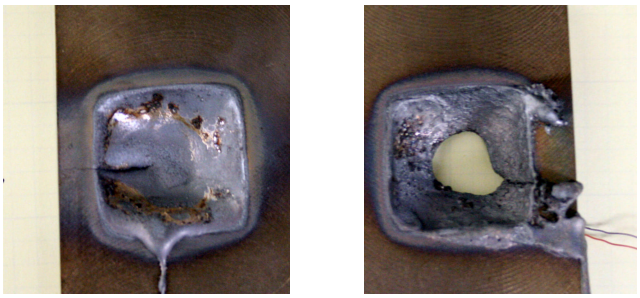

Fig. 2. Iron coupons after irradiation experiments. Left: no flow; right: airflow. The beam spot size is 3x3 cm^2.

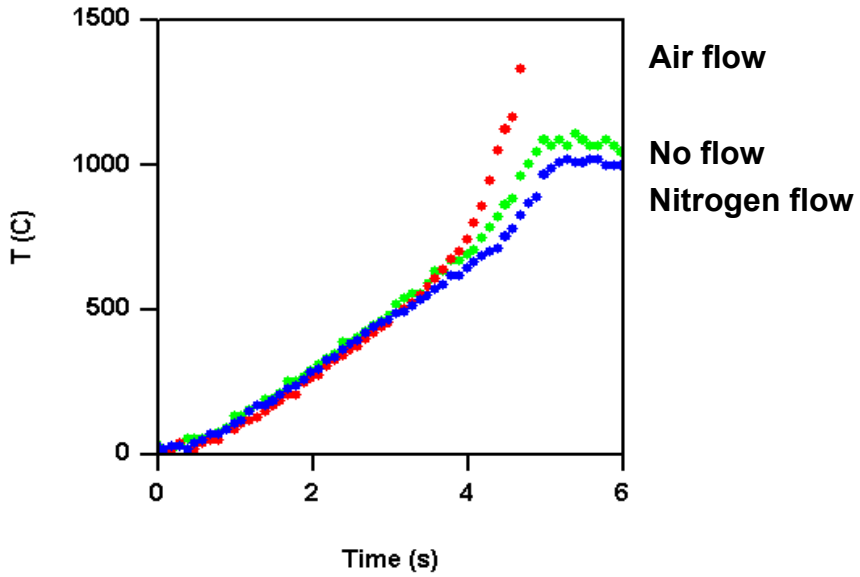

Fig. 3. Thermocouple readings for the iron coupons. The beam was turned off at 5 s. The data have a maximum jitter about the mean of about 10 deg.

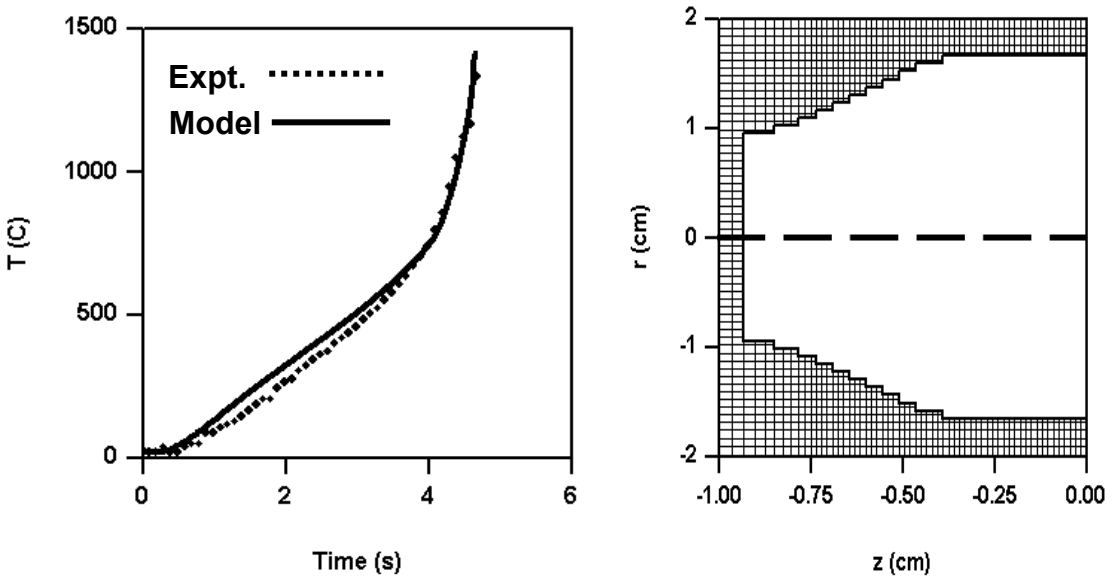

Fig. 4. Left: Comparison of experimental and calculated temperatures on the rear center of an iron coupon, with airflow. Right: Calculated hole profile immediately before breakthrough. A circularly symmetric geometry is used.

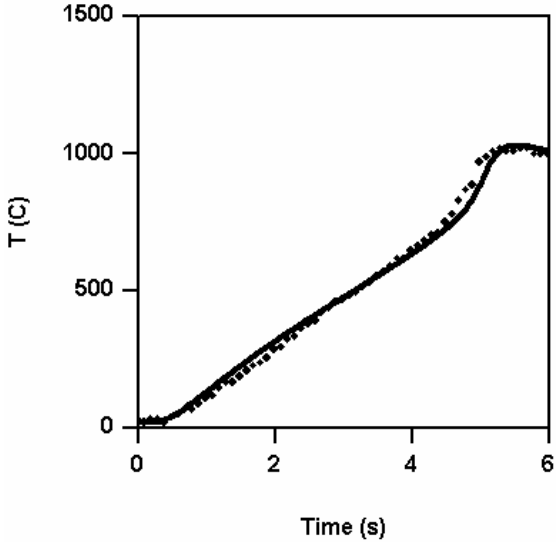

Fig. 5. Comparison of experimental and calculated temperatures on the rear center of an iron coupon, with nitrogen flow.

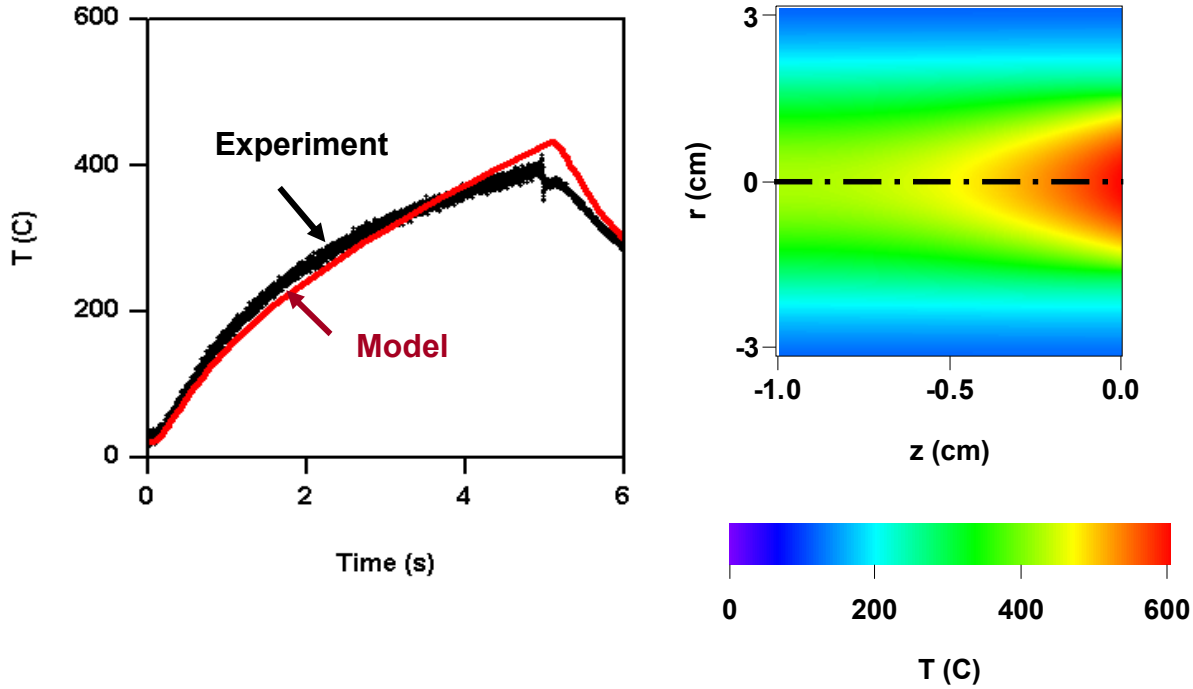

Fig. 6. Irradiation of a 1-cm aluminum coupon by 25 kW for 5 s, with a spot size of 2.8x2.8 cm^2. Left: Temperature trace of a thermocouple on the rear center, along with the model calculation. Right: Calculated temperature distribution immediately before the beam is turned off (the beam enters from the right).

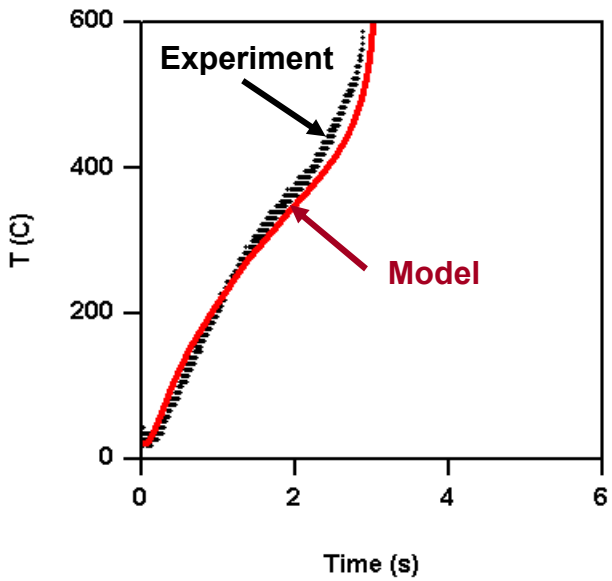

Fig. 7. Temperature trace at the rear center of an aluminum coupon, during irradiation with a spot size of 2x2 cm^2.

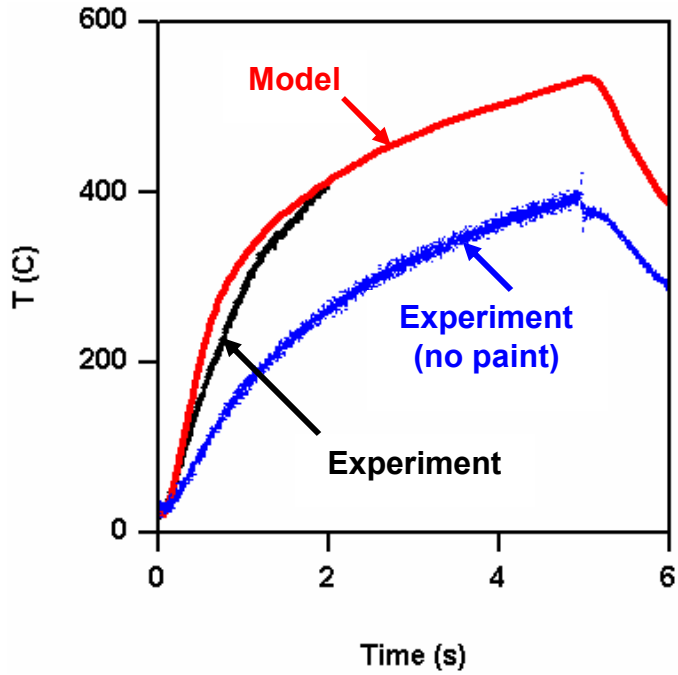

Fig. 8. Black line: Thermocouple trace for the irradiation of a 1-cm painted aluminum coupon by 25 kW for 5 s, with a spot size of 3x3 cm^2 (black line). The thermocouple failed at 2 s. The red line gives the model prediction. The blue line gives the temperature trace for a 2.8x2.8 cm^2 spot with no paint, from Fig. 6.